2013 American Control Conference (ACC)
Washington, DC, USA, June 17-19, 2013

Models and Methodology for Optimal Vehicle Maneuvers Applied to a Hairpin Turn

Karl Berntorp, Björn Olofsson and Bo Bernhardsson
Department of Automatic Control,
Lund University, SE–221 00 Lund, Sweden
firstname.lastname@control.lth.se

Kristoffer Lundahl and Lars Nielsen
Department of Electrical Engineering,
Linköping University, SE–581 83 Linköping, Sweden
firstname.lastname@liu.se

***Abstract*—There is currently a strongly growing interest in obtaining optimal control solutions for vehicle maneuvers, both in order to understand optimal vehicle behavior and to devise improved safety systems, either by direct deployment of the solutions or by including mimicked driving techniques of professional drivers. However, it is nontrivial to find the right mix of models, formulations, and optimization tools to get useful results for the above purposes. Here, a platform is developed based on a state-of-the-art optimization tool together with adoption of existing vehicle models, where especially the tire models are in focus. A minimum-time formulation is chosen to the purpose of gaining insight in at-the-limit maneuvers, with the overall aim of possibly finding improved principles for future active safety systems. We present optimal maneuvers for different tire models with a common vehicle motion model, and the results are analyzed and discussed. Our main result is that a few-state single-track model combined with different tire models is able to replicate the behavior of experienced drivers. Further, we show that the different tire models give quantitatively different behavior in the optimal control of the vehicle in the maneuver.**

I. Introduction

Optimization of vehicle trajectories can be motivated from different perspectives. One objective is to develop improved active safety systems for standard customer cars. The Electronic Stability Program (ESP) systems, see [1] and [2], of today are still behind the maneuvering performance achievable by professional race car drivers in critical situations, but the vision for improvement is there, see [3]. A recent survey on optimal control in automotive applications [4] points out:

> Most often, the optimal control itself will be interesting mainly insofar as it enables the discovery of the best possible system performance. Occasionally, the optimal control will provide a basis for the design and operation of practical systems.

Further, the survey points out that finding the right balance between models, correct formulations, and optimization methods is nontrivial, and that the state-of-the-art today is hampered by long simulation runs. The goal in this paper, regarding methodology, is to develop and investigate a platform for useful solutions to these problems.

It is a common observation that the criterion of time-optimality in aggressive vehicle maneuvers, combined with input and state constraints, often results in control signals using the extremal cases of the input and state regions. It is therefore crucial how, *e.g.*, the tires are modeled outside their normal range of operation.

Fig. 1. An example of a hairpin turn. Photo courtesy of RallySportLive.

The interaction between tire and road is complex, and different tires have different characteristics. Even when only considering the longitudinal stiffness, the experimental values differ considerably between tires, and the variability can typically be 20–100 %, see [5]. Further, in addition to the differences in stiffness—*i.e.*, the slope of the longitudinal force-slip curve—there are also differences between the characteristic shape of the curve at the maximum force, where the peak can be more or less accentuated. This is illustrated for Pacejka's Magic Formula and the HSRI model in [5]. The complete tire model capturing both longitudinal and lateral forces can thus be expected to have large variability both in shape, parameters, and parameter irregularity.

The control oriented goal of this paper is to find a formulation that gives insight into improved safety systems; *e.g.*, future ESP systems performing closer to what the most experienced drivers can do. To that end we study a time-optimal maneuver in a hairpin turn, an interesting situation testing the limits of maneuverability of a car in a certain situation. In [6] we reported that simplified vehicle models identified from experimental data managed to replicate the behavior of real vehicles. However, this was based on less aggressive driving situations, and not using optimization. Previous work in the subject of optimal control of vehicles in certain time-critical situations such as T-bone collisions and cornering can be found in, *e.g.*, [7], [8], [9]. In [10], [11], methods for constraint-based trajectory planning for optimal maneuvers are presented. Further, the papers [12], [13] discuss optimal control of over-

actuated vehicles, where similar optimization tools as those used in the present paper are utilized.

This paper is outlined as follows: The problem description and overall aim of the paper are discussed in Sec. II. Vehicle and tire modeling and the specific models investigated in this study are presented in Sec. III, followed by the formulation and solution of the studied time-optimal maneuvering problem in Sec. IV. Optimization results and a subsequent discussion of the obtained results are provided in Sec. V. Finally, conclusions and aspects on future work are given in Sec. VI.

II. Problem description

The goal of the work presented in this paper is twofold. The first goal is to find the time-optimal vehicle trajectory when maneuvering through a hairpin turn, see Fig. 1 for an example, with the vehicle being subject to various constraints.

Another aim of the study is to explore whether different vehicle models yield fundamentally different solutions, not only in the cost function but also in the internal behavior of the vehicle. Hence, a part of the work is devoted to investigating how the models differ. We consider differential-algebraic models of the form

$$\begin{aligned} \dot{x}(t) &= G(x(t), y(t), u(t)), \\ 0 &= h(x(t), y(t), u(t)), \end{aligned}$$

where $G(x(t), y(t), u(t))$ and $h(x(t), y(t), u(t))$ are twice continuously differentiable nonlinear functions of the vehicle differential variables x, algebraic variables y, and control inputs u. The models used are based on the same vehicle model, but differ in the tire modeling aspects.

The motivation for the twofold goal is that, to the best of our knowledge, most model comparisons in literature are based on simulation rather than optimization. Since time-optimal optimization problems tend to push the vehicle more to the extremes than simulations do, it is plausible that different conclusions about model behavior can be made from such an analysis.

III. Modeling

The vehicle dynamics modeling in this section incorporates the vehicle motion modeling and the tire force modeling, with emphasis on the latter. Further, calibration of the tire models is discussed and a subsequent investigation of the qualitative behavior of the models studied is presented.

A. Vehicle Modeling

As a basis for the vehicle dynamics model, a two-dimensional single-track model, with two translational and one rotational degrees-of-freedom, was used, see Fig. 2. The motion equations are expressed by, see [14], [15],

$$\dot{v}_x - v_y\dot{\psi} = \frac{1}{m}(F_{x,f}\cos(\delta) + F_{x,r} - F_{y,f}\sin(\delta)), \quad (1)$$

$$\dot{v}_y + v_x\dot{\psi} = \frac{1}{m}(F_{y,f}\cos(\delta) + F_{y,r} + F_{x,f}\sin(\delta)), \quad (2)$$

$$I_z\ddot{\psi} = l_f F_{y,f}\cos(\delta) - l_r F_{y,r} + l_f F_{x,f}\sin(\delta), \quad (3)$$

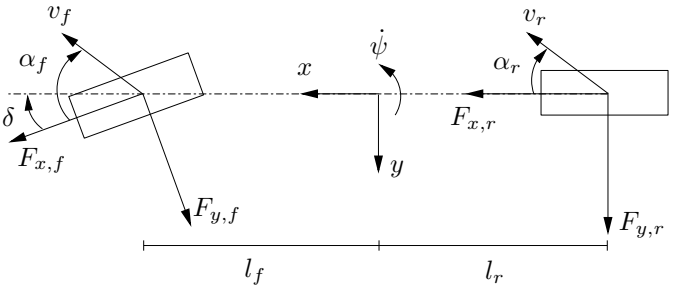

Fig. 2. The single-track model considered in this paper.

TABLE I
Vehicle model parameters used in (1)–(10).

Notation	Value	Unit
l_f	1.3	m
l_r	1.5	m
m	2100	kg
I_z	3900	kgm^2
R_e	0.3	m
R_w	0.3	m
I_w	4.0	kgm^2
g	9.82	ms^{-2}

where m is the vehicle mass, I_z is the vehicle inertia, $\dot{\psi}$ is the yaw rate, δ is the steering wheel angle, $v_{x,y}$ are the longitudinal and lateral velocities, $l_{f,r}$ are the distances from center-of-gravity to the front and rear wheel base, and $F_{x,y}$ are the longitudinal and lateral forces acting on the front and rear wheels. The slip angles, $\alpha_{f,r}$, and slip ratios, $\kappa_{f,r}$, are described by

$$\alpha_f = \delta - \arctan\left(\frac{v_y + l_f\dot{\psi}}{v_x}\right), \quad (4)$$

$$\alpha_r = -\arctan\left(\frac{v_y - l_r\dot{\psi}}{v_x}\right), \quad (5)$$

$$\kappa_f = \frac{R_e\omega_f - v_{x,f}}{v_{x,f}}, \quad (6)$$

$$\kappa_r = \frac{R_e\omega_r - v_{x,r}}{v_{x,r}}, \quad (7)$$

$$v_{x,f} = v_x\cos(\delta) + (v_y + l_f\dot{\psi})\sin(\delta), \quad (8)$$

$$v_{x,r} = v_x, \quad (9)$$

where R_e is the effective wheel radius and $\omega_{f,r}$ are the front and rear wheel angular velocities. The wheel dynamics, necessary for slip ratio computation, is given by

$$T_i - I_w\dot{\omega}_i - F_{x,i}R_w = 0\ , \quad i = f, r. \quad (10)$$

Here, T_i is the driving/braking torque, I_w is the wheel inertia, and R_w is the loaded wheel radius. The numerical values for the vehicle model parameters used in this study are provided in Table I.

B. Tire Modeling

When developing a platform for investigation of optimal maneuvers, it is of interest to be able to handle and compare

different tires, and thus to cope with different tire models. We have considered two different model categories for tire modeling, whose characteristics are described next.

The nominal tire forces—*i.e.*, the forces under pure slip conditions—are computed with the Magic Formula model [16], given by

$$F_{x0,i} = \mu_x F_{z,i} \sin(C_{x,i} \arctan(B_{x,i}\kappa_i)), \quad (11)$$
$$F_{y0,i} = \mu_y F_{z,i} \sin(C_{y,i} \arctan(B_{y,i}\alpha_i)), \quad (12)$$
$$F_{z,i} = mg(l - l_i)/l, \ i = f, r. \quad (13)$$

In (11)–(13), μ_x and μ_y are the friction coefficients, B and C are model parameters, $l = l_f + l_r$, and g is the constant of gravity .

Under combined slip conditions—*i.e.*, both κ and α are nonzero—the longitudinal and lateral tire forces will depend on both slip quantities. How this coupling is described can have immense effect on the vehicle dynamics. In an optimal maneuver, the solution will use the best combination of longitudinal and lateral force, and these forces are, of course, coupled via the physics of the tire. In order to compare different models, plotting of the resulting tire force is illustrative, *c.f.* Figs. 3–6, to visualize the interaction between longitudinal and lateral force.

Even though detailed experiments, like the ones in [5] for longitudinal stiffness, are lacking for the complete longitudinal-lateral tire interaction, there is a vast plethora of characteristics, see [1], [16], [17], and [18]. We have chosen two different tire models for our study, described below.

1) Friction Ellipse: A common way to model combined slip is to use the friction ellipse, described by

$$F_{y,i} = F_{y0,i}\sqrt{1 - \left(\frac{F_{x0,i}}{\mu_x F_{z,i}}\right)^2}, \quad (14)$$

where F_x is used as an input variable. However, we have opted for using the driving/braking torques as input, see (10), since this is a quantity that can be controlled in a physical setup of a vehicle.

2) Weighting Functions: Another approach described in [16] is to scale the nominal forces, (11)–(12), with weighting functions, $G_{x\alpha,i}$ and $G_{y\kappa,i}$, which depend on α and κ. The relations in the x-direction are

$$B_{x\alpha,i} = B_{x1,i} \cos(\arctan(B_{x2,i}\kappa_i)), \quad (15)$$
$$G_{x\alpha,i} = \cos(C_{x\alpha,i} \arctan(B_{x\alpha,i}\alpha_i)), \quad (16)$$
$$F_{x,i} = F_{x0,i} G_{x\alpha,i}. \quad (17)$$

The corresponding relations in the y-direction are given by

$$B_{y\kappa,i} = B_{y1,i} \cos(\arctan(B_{y2,i}(\alpha_i - B_{y3,i}))), \quad (18)$$
$$G_{y\kappa,i} = \cos(C_{y\kappa,i} \arctan(B_{y\kappa,i}\kappa_i)), \quad (19)$$
$$F_{y,i} = F_{y0,i} G_{y\kappa,i}. \quad (20)$$

C. Calibrating Tire Models for Comparison

When comparing an optimal maneuver based on two different tire models, it is not obvious how to calibrate the models to get comparable solutions. For example, in Fig. 3 and Fig. 6 we show two different types of tire models. In order to equalize these models in comparative studies, one way would be to have the same average resultant force, whereas another way would be to equalize the longitudinal stiffness. In this study, the same parameters have been used for the nominal lateral force; *i.e.*, the lateral force characteristics are the same for all models when considering pure lateral slip.

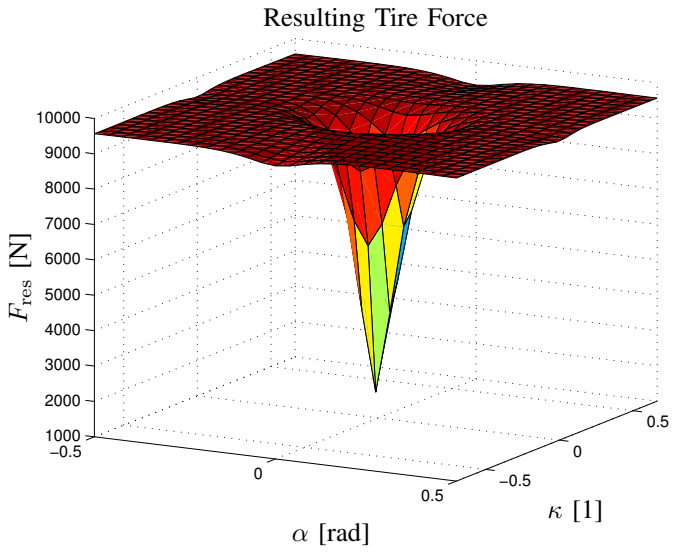

Fig. 3. Resultant tire force F_{res} for a friction ellipse model parametrized to give isotropic behavior.

D. Qualitative Behavior of Tire Models

In Figs. 3–6 it is shown how the resulting force, defined by

$$F_{\text{res}} = \sqrt{F_{x,i}^2 + F_{y,i}^2}, \ i = f, r,$$

for the above tire models varies over slip angle and slip ratio with the parameters presented in Table II. Studying Figs. 3–6 gives a basis for discussion of the behavior of the tire models in an optimal maneuver.

Figure 3 displays the friction ellipse model, and Fig. 4 shows the weighting functions model for an isotropic parametrization. These are both considered isotropic in the sense that they have the same properties in the lateral and longitudinal directions. The most obvious difference in these figures can be seen for large slip angles, where an increase in the slip ratio will increase the resulting force for the friction ellipse model and, on the contrary, decrease it for the model based on weighting functions.

In contrast, considering the nonisotropic models, Figs. 5 and 6, different force characteristics are obtained in the longitudinal and lateral directions. The model based on the weighting functions is parametrized according to the Pacejka model in [16], thus representing a realistic tire behavior. The friction ellipse model also uses the Pacejka parameters in [16] for the nominal tire forces. Hence, both of the nonisotropic models will exhibit equivalent tire characteristics for pure

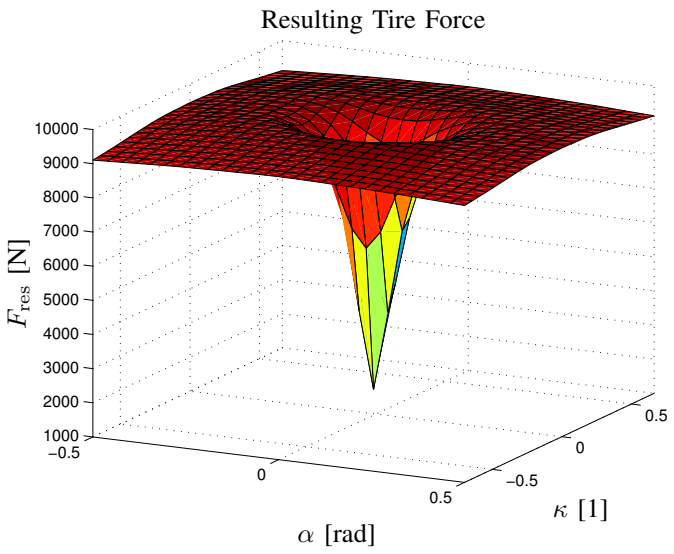

Fig. 4. Resultant tire force F_{res} for a weighting functions model parametrized to give isotropic behavior.

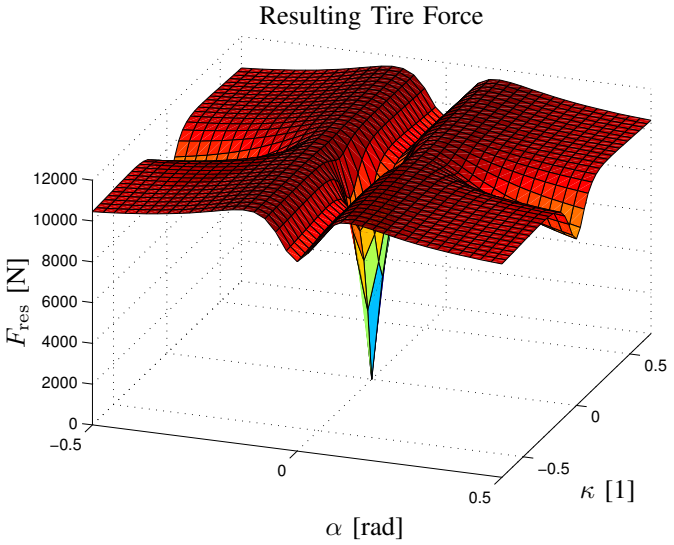

Fig. 5. Resultant tire force F_{res} with a friction ellipse model with experimental parameters from [16] ($\mu_x = 1.2,\ \mu_y = 1.0$).

slip conditions. Further, the characteristic peaks in F_{res}—not visible in the isotropic models—influence the behavior of the tire force model significantly.

IV. Optimization

Based on the dynamics described in the previous section, the time-optimal maneuver for the hairpin turn is to be determined. This is expressed as an optimization problem, and, considering the physical setup of the problem, it is clear that an optimal solution exists. The resulting optimization problem is more challenging than thought at first sight, since the time-optimality implies that the tire friction model operates on the boundary of its validity. Also, solving dynamic optimization problems where the final time is free, is more demanding than

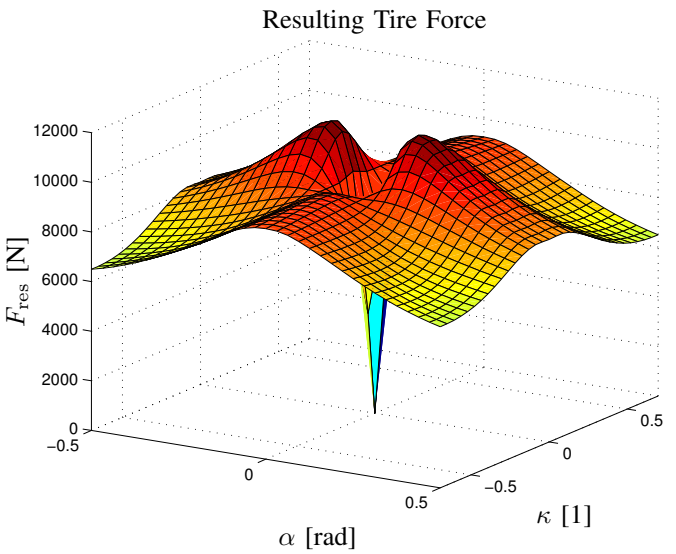

Fig. 6. Resultant tire force F_{res} for a weighting functions model with the same friction coefficients as in Fig. 5.

TABLE II
Tire model parameters for friction ellipse with isotropic behavior (FE-Iso), nonisotropic behavior (FE-Noniso), and weighting functions with isotropic behavior (WF-Iso), nonisotropic behavior (WF-Noniso).

Parameter	FE-Iso	FE-Noniso	WF-Iso	WF-Noniso
μ_x	1.0	1.2	1.0	1.2
μ_y	1.0	1.0	1.0	1.0
$C_{\alpha,f}$	1.09e5	1.09e5	1.09e5	1.09e5
$C_{\alpha,r}$	1.02e5	1.02e5	1.02e5	1.02e5
$C_{\kappa,f}$	1.09e5	2.38e5	1.09e5	2.38e5
$C_{\kappa,r}$	1.02e5	2.06e5	1.02e5	2.06e5
C_x	1.3	1.7	1.3	1.7
C_y	1.3	1.3	1.3	1.3
$B_{x1,f}$	-	-	8.55	11.23
$B_{x2,f}$	-	-	8.33	10.80
$C_{x\alpha,f}$	-	-	1.03	1.14
$B_{y1,f}$	-	-	8.63	6.37
$B_{y2,f}$	-	-	8.35	2.64
$B_{y3,f}$	-	-	0	0
$C_{y\kappa,f}$	-	-	1.03	1.03
$B_{x1,r}$	-	-	9.28	11.71
$B_{x2,r}$	-	-	9.04	11.61
$C_{x\alpha,r}$	-	-	1.03	1.14
$B_{y1,r}$	-	-	9.38	5.88
$B_{y2,r}$	-	-	9.08	2.98
$B_{y3,r}$	-	-	0	0
$C_{y\kappa,r}$	-	-	1.02	1.08

a problem with fixed end time. Further, we have found that numerical issues easily arise and that the optimization does not converge without proper initialization. In order to make the convergence more robust from a numerical point of view, scaling of the optimization variables is essential.

A. Formulation of Optimization Problem

Consider the time horizon $t \in [0, t_f]$, where t_f is the free final time to be determined as part of the solution procedure. Express the vehicle dynamics (1)–(3) and (10) as $\dot{x}(t) = G(x, y, u)$, where x are the differential variables and y

are the algebraic variables. The wheel driving/braking torques $T = \begin{pmatrix} T_f & T_r \end{pmatrix}$ and the steering angle δ are considered as the input variables, $u = (T \quad \delta)^{\mathrm{T}}$. Further, express (4)–(9), (11)–(13), and (14) or (15)–(20), depending on the friction model considered, as $0 = h(x, y, u)$. The dynamic optimization problem to be solved can then be stated as follows:

$$\begin{aligned}
\text{minimize} \quad & t_f && (21)\\
\text{subject to} \quad & T_{i,\min} \le T_i \le T_{i,\max}, \ i = f, r && (22)\\
& |\delta| \le \delta_{\max}, \quad |\dot{\delta}| \le \dot{\delta}_{\max} && (23)\\
& |F_{x,i}| \le F_{x,i,\max}, \ i = f, r && (24)\\
& |F_{y,i}| \le F_{y,i,\max}, \ i = f, r && (25)\\
& \left(\frac{X_p}{R_1^i}\right)^6 + \left(\frac{Y_p}{R_2^i}\right)^6 \ge 1 && (26)\\
& \left(\frac{X_p}{R_1^o}\right)^6 + \left(\frac{Y_p}{R_2^o}\right)^6 \le 1 && (27)\\
& x(0) = x_0, \quad y(0) = y_0 && (28)\\
& x(t_f) = x_{t_f}, \quad y(t_f) = y_{t_f} && (29)\\
& \dot{x}(t) = G(x, y, u), \quad 0 = h(x, y, u), && (30)
\end{aligned}$$

where (x_0, y_0) are the initial conditions for the differential/algebraic variables, (x_{t_f}, y_{t_f}) are the desired values at the final time $t = t_f$, and (X_p, Y_p) is the position of the center-of-gravity of the vehicle. Note that the path constraint is formulated using super-ellipses and the shape of the path is determined by the radii R_1^i, R_2^i, R_1^o, and R_2^o.

B. Solution of Optimization Problem

Because of the complex nature of the nonlinear and non-convex optimization problem in (21)–(30), analytical solutions are intractable. Instead, we utilize numerical methods based on simultaneous collocation [19]. Direct collocation is used, where all state and input variables, originally described in continuous time, are discretized prior to the optimization. This results in a discrete-time nonlinear program (NLP). The collocation procedure transforms the original infinite-dimensional problem to a finite-dimensional problem with a large, however finite, number of optimization variables, on which numerical optimization methods are applied.

C. Implementation and Solution

The vehicle and tire dynamics are implemented using the modeling language Modelica [20]. Utilizing Optimica [21], which is an extension of Modelica for high-level description of optimization problems based on Modelica models, the implementation of the vehicle and tire dynamics described in Sec. III and the optimal control problem is straightforward.

The collocation procedure and solution of the optimization problem are performed using the open-source software platform JModelica.org [22], [23]. In JModelica.org, orthogonal collocation is implemented, where Lagrange polynomials are used for representation of the state profiles in each element and the location of the collocation points are chosen as the corresponding Radau points. The resulting NLP is solved internally using the numerical solver Ipopt [24], which is a solver based on interior-point methods opted for large, but sparse, optimization problems.

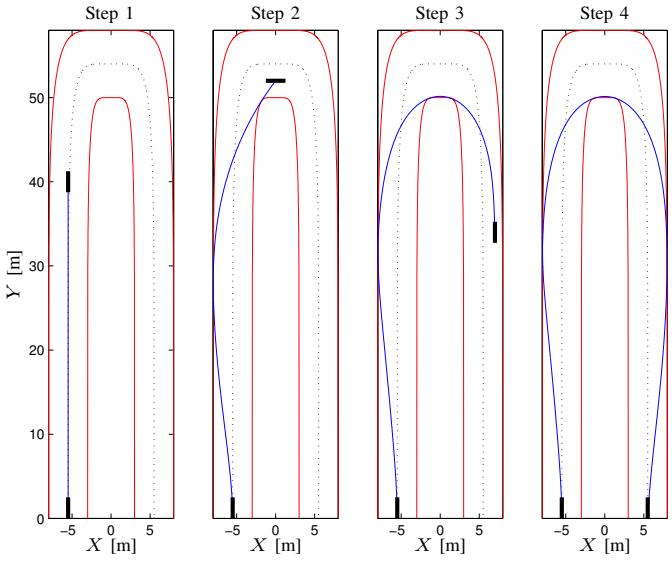

Fig. 7. Initialization procedure for solving the time-optimal hairpin turn maneuver problem. The whole problem is solved by stepwise solving four successive problems. The black rectangles in the figure indicate the position and direction of the vehicle at the initial and final state in each problem.

D. Initialization Procedure

Robust convergence to a solution of the NLP in Ipopt relies on proper initialization. Two approaches are available to this purpose: Simulation of an initial guess using driver models and division of the problem into smaller subproblems, respectively. In this paper, the latter approach is utilized. Consequently, the hairpin turn problem is solved in four steps, see Fig. 7. The results from the solution of each subproblem is used for initialization of the subsequent problem. Hence, the final optimal maneuver is determined stepwise.

V. Results

For the evaluations we set the maximum allowed wheel angle, δ, and wheel-angle change rate, $\dot{\delta}$, to 30 deg and 60 deg/s, respectively, which are reasonable parameters, both seen from physical and driver limitations. Also, constraints on the driving/braking torques and tire forces were introduced:

$$\begin{aligned}
T_f &\le 0, && (31)\\
T_f &\ge -\mu_x F_{z,f} R_w, && (32)\\
|T_r| &\le \mu_x F_{z,r} R_w, && (33)\\
|F_{x,i}| &\le \mu_x F_{z,i}, \ i = f, r, && (34)\\
|F_{y,i}| &\le \mu_y F_{z,i}, \ i = f, r. && (35)
\end{aligned}$$

We let the road be 5 m wide. Further, the start, (X_p^0, Y_p^0), and final vehicle position, $(X_p^{t_f}, Y_p^{t_f})$, were set to be in the middle of the road. The initial velocity was $v_0 = 25$ km/h. Figures 8–11 show the vehicle trajectory together with the most relevant states for all four models. Note that the vehicle is rear-wheel driven. All models have similarities: The vehicle starts with

giving full engine torque while turning to allow for wider curve taking. When entering the curve the vehicle starts to break with both wheels, which it does approximately until reaching the half-way point. Furthermore, all models give rise to vehicle slip. The trajectory plots show that the slip—*i.e.*, the angle between the velocity vector and the longitudinal direction of the vehicle—is significant, exceeding 30 deg in the most critical parts of the maneuver. The maneuvering achieving this behavior is very similar to drifting techniques, where the rear wheel driving/braking torque is used to control the rear lateral tire force. The front wheels are only controlled with the steering angle, utilizing counter steering if necessary. Also, the qualitative slip behavior is congruent with the driving behavior often seen when rally drivers perform similar maneuvers, indicating that the obtained optimization results manage to replicate behavior utilized in reality. Furthermore, it also shows that even a few-state single-track model using the friction ellipse for tire modeling manages to capture fundamental and relevant behavior, even for minimum-time optimization problems.

For the four parameter sets in Table II, the final time values are for the respective column: $t_f \approx 8.82$, $t_f \approx 8.42$, $t_f \approx 8.80$, and $t_f \approx 8.44$. Hence, the objective function, t_f, deviates approximately 0.4 s when comparing all four model configurations. Comparing the isotropic and nonisotropic models, the deviation in final time between the friction ellipse model and the weighting functions model is less than 0.02 s.

A. Comparison of Isotropic Models

Studying the obtained results closer, we see that Figs. 8 and 9 only have minor differences, if any. This should, of course, come as no surprise since the two models are parametrized to be isotropic, *c.f.* Figs. 3–4. This is a verification that the optimization tool is able to handle both of these models, and also that two completely different model categories, parametrized to achieve equivalent resultant force characteristics, give similar results for the optimal maneuver. Figures 12 and 13 show the force trajectories as functions of α and κ, corresponding to Figs. 8 and 9. By inspection we note that the α and κ trajectories, and consequently the resulting tire force trajectory, vary more for the rear wheels, which is caused by the vehicle being rear-wheel driven. Further, when comparing the force curves for the rear wheel it is clear that the friction ellipse model seems to penalize combined slip more throughout the turn. This can be explained by that the lateral tire force decreases faster with increasing slip ratio for the friction ellipse than for the weighting functions model. For example, when the longitudinal force approaches its maximum value, the lateral force tends to zero. For the corresponding slip ratio, the weighting functions model predicts a larger lateral force than the friction ellipse model does.

B. Comparison of Nonisotropic Models

When investigating Figs. 10 and 11 we see that there are fundamental differences. First, the maximum steering angle, δ, in Fig. 11 is twice as large as δ in Fig. 10. Second, the maximum yaw rate is larger for the weighting functions model, see Fig. 11, but the yaw rate when in the turn (between $t \approx 3.5$–4.5 s) is smaller. Third, the weighting functions model seldom uses the rear wheel for braking. Rather, it maximizes the braking force on the front wheel instead of distributing the braking force to both wheels. We believe that this behavior stems from that the weighting functions model provide, in addition to the low-slip solution, a large-slip alternative—*i.e.*, does not penalize combined slip—for a given resulting force. The force trajectories in Figs. 14 and 15 verify this claim. These observations indicate that this behavior is model

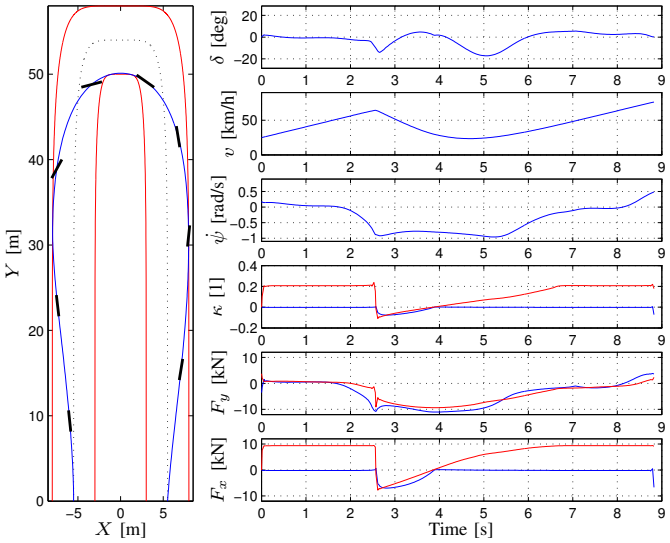

Fig. 8. Optimization result for friction ellipse model with isotropic behavior with parameters as in column two in Table II. In the κ, F_x, and F_y plots the blue curves visualize the front wheel and the red curves the rear wheel. The black rectangles in the XY-trajectory plot show the sideslip angle each second of the maneuver.

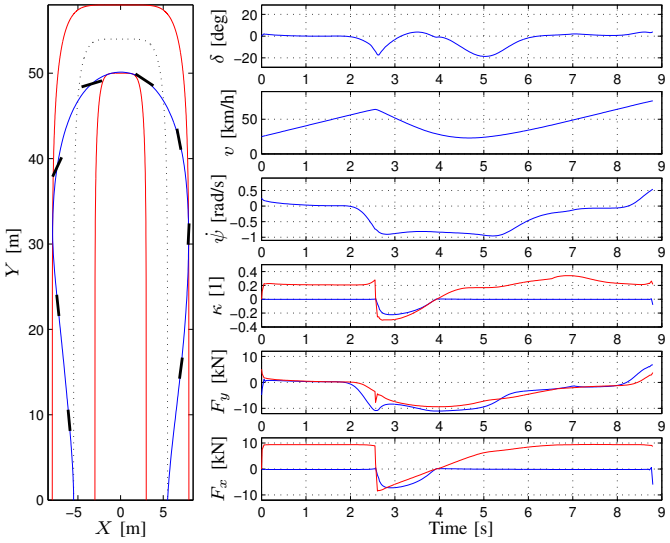

Fig. 9. Optimization result for weighting functions model with isotropic behavior with parameters as in column four in Table II. Same notation and colors as in Fig. 8.

dependent rather than parameter dependent.

Another interesting behavior can be seen when studying the slip ratios, κ. For the weighting functions model, a large peak occurs when increasing the yaw rate at $t \approx 2.3$ s. At this stage, when trying to turn quickly, it is desired to have a small lateral force at the rear, which, in the weighting functions model, can be achieved by increasing the slip ratio as much as possible. In the isotropic weighting functions model, this tendency can also be seen. However, since the force decrease in the longitudinal direction is comparatively small, only a modest peak in the slip ratio appears. Studying the friction ellipse model instead, no such peak in slip ratio can be seen. Also, the friction ellipse model as it is implemented here, will increase the lateral force if the slip ratio exceeds the maximum longitudinal force.

C. Comparing the Isotropic and Nonisotropic Models

When comparing the friction ellipse model for the two different parameter sets—*i.e.*, Figs. 8 and 10—we note a couple of discrepancies. The peak of δ is more accentuated in Fig. 10. Also, the longitudinal force, and thereby the longitudinal velocity, is larger in magnitude. This is attributed to the larger longitudinal friction coefficient, μ_x, see Table II. This, in turn, is a result of the fitting procedure used, described in Sec. III-C. The difference in steering angle can, most probably, also be deduced to this, since a larger velocity will demand more aggressive steering to counteract the larger forces. When comparing the force trajectories for the same models, Figs. 12 and 14, we see that they are very similar.

The weighting functions have more pronounced differences: First, δ in Fig. 9 hardly exceeds 0 rad. Moreover, the yaw rate is larger in Fig. 11. Third, the forces differ significantly. Partly, the differences can be attributed to the difference in longitudinal friction coefficient. We believe that a contributor is the significant differences between the maxima and minima in Fig. 15.

VI. Conclusions and Future Work

This paper aimed at using vehicle and tire models frequently encountered in literature to give insight into improved safety systems. We presented a comparison of vehicle behavior for minimum-time optimization of a hairpin maneuver, where different tire models were used. We exploited a single-track model for vehicle modeling. Although the results differed in some respects, the qualitative behavior was similar for all models. We showed that even a few-state single-track model using the friction ellipse for tire modeling managed to capture fundamental and relevant behavior. This implies that for future optimization-based safety systems rather simple models may suffice. However, the friction ellipse model and weighting functions model showed some dissimilarities; *e.g.*, the braking behavior was different. This might have impact on model choice, especially considering safety systems such as yaw rate controllers where the brakes typically are the actuators.

For the future we plan to do a similar investigation for different tires and surfaces, which provides insight into optimal control of maneuvers under different road conditions. Further,

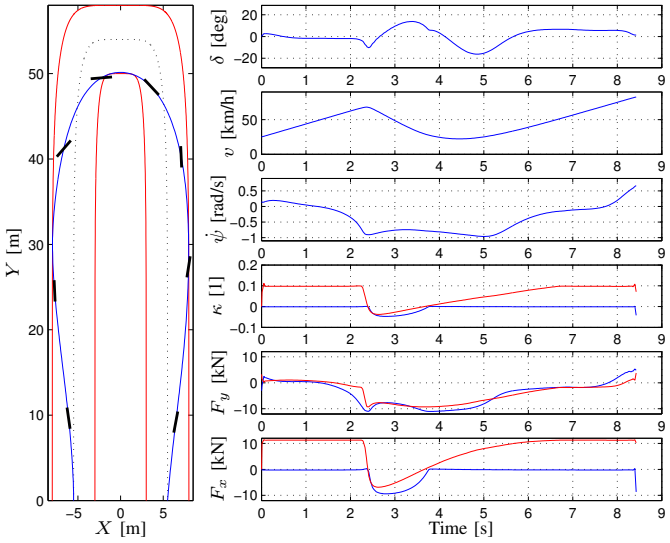

Fig. 10. Optimization results for friction ellipse model with parameters as in column three in Table II. Same notation and colors as in Fig. 8.

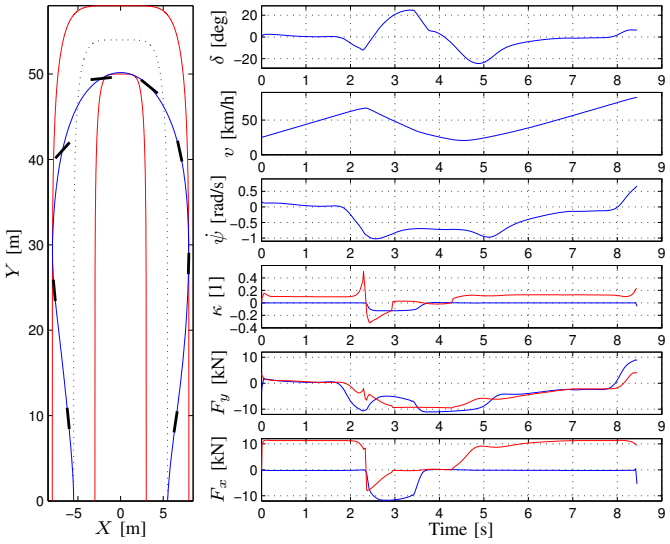

Fig. 11. Optimization results for weighting functions model with parameters as in column five in Table II. Same notation and colors as in Fig. 8.

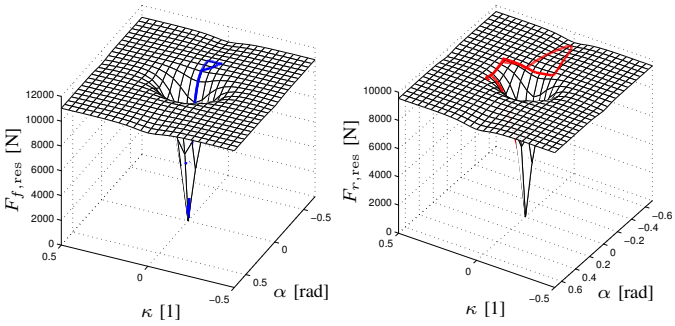

Fig. 12. 3D plot of force curve for friction ellipse model with isotropic behavior corresponding to Fig. 8. Blue (front wheel) and red curves (rear wheel) are the trajectories generated by optimization.

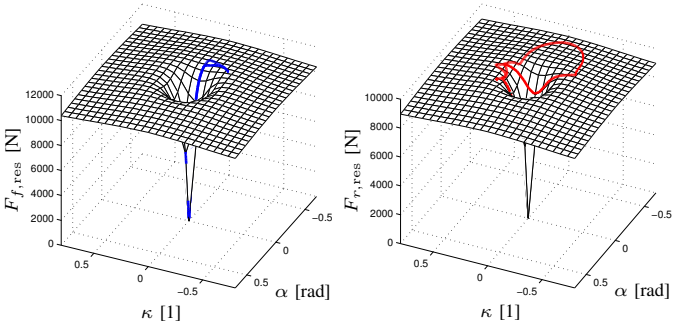

Fig. 13. 3D plot of force curve for weighting functions model with isotropic parameters corresponding to Fig. 9.

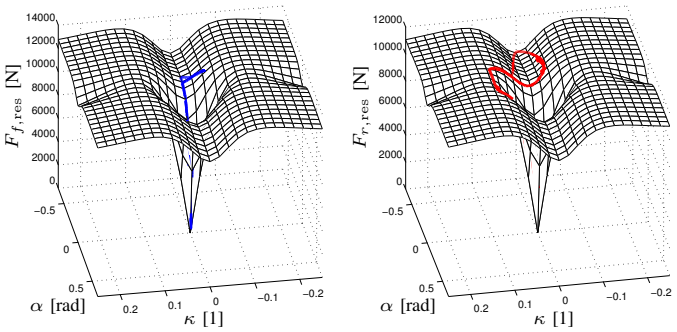

Fig. 14. 3D plot of force curve for friction ellipse model with parameters corresponding to Fig. 10.

investigating optimal path tracking is a natural extension of the work presented in this paper; in this context other optimization criteria than time-optimality, such as deviation from the specified path or energy consumption, are of interest.

ACKNOWLEDGMENTS

This work has been supported by ELLIIT, the Strategic Area for ICT research, funded by the Swedish Government.

K. Berntorp, B. Olofsson, and B. Bernhardsson are members of the LCCC Linnaeus Center at Lund University, supported by the Swedish Research Council.

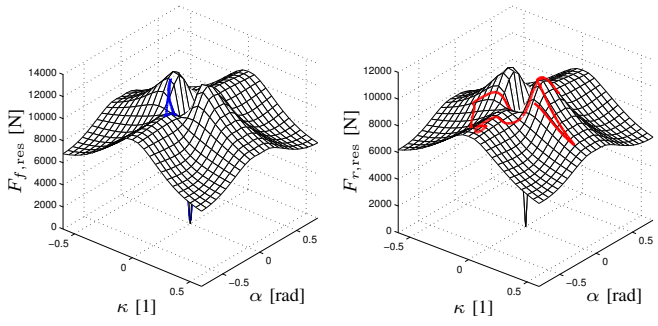

Fig. 15. 3D plot of force curve for weighting functions model with parameters corresponding to Fig. 11.

REFERENCES

[1] R. Isermann, *Fahrdynamik-Regelung: Modellbildung, Fahrerassistenzsysteme, Mechatronik*. Wiesbaden, Germany: Vieweg-Verlag, 2006.

[2] K. Liebemann, K. Meder, J. Schuh, and G. Nenninger, "Safety and performance enhancement: The Bosch electronic stability control," 2005, Paper Number 05-0471m, Robert Bosch GmbH.

[3] J. Funke, P. Theodosis, R. Hindiyeh, G. Stanek, K. Kritatakirana, C. Gerdes, D. Langer, M. Hernandez, B. Muller-Bessler, and B. Huhnke, "Up to the limits: Autonomous Audi TTS," in *IEEE Intelligent Vehicles Symp.*, Alcalá de Henares, Spain, June 2012, pp. 541–547.

[4] R. S. Sharp and H. Peng, "Vehicle dynamics applications of optimal control theory," *Vehicle System Dynamics*, vol. 49, no. 7, pp. 1073–1111, 2011.

[5] C. Carlson and J. Gerdes, "Consistent nonlinear estimation of longitudinal tire stiffness and effective radius," *IEEE Trans. Control Syst. Technol.*, vol. 13, no. 6, pp. 1010–1020, Nov. 2005.

[6] K. Lundahl, J. Åslund, and L. Nielsen, "Investigating vehicle model detail for close to limit maneuvers aiming at optimal control," in *22nd Int. Symp. on Dynamics of Vehicles on Roads and Tracks (IAVSD)*, Manchester, United Kingdom, 2011.

[7] I. Chakraborty, P. Tsiotras, and J. Lu, "Vehicle posture control through aggressive maneuvering for mitigation of T-bone collisions," in *IEEE Conf. on Decision and Control (CDC)*, Orlando, FL, 2011, pp. 3264–3269.

[8] E. Velenis and P. Tsiotras, "Minimum time vs. maximum exit velocity path optimization during cornering," in *IEEE Int. Symp. on Industrial Electronics (ISIE)*, Dubrovnik, Croatia, June 2005, pp. 355–360.

[9] E. Velenis, "FWD vehicle drifting control: The handbrake-cornering technique," in *IEEE Conf. on Decision and Control (CDC)*, Orlando, FL, 2011, pp. 3258–3263.

[10] S. Anderson, S. Peters, T. Pilutti, and K. Iagnemma, "An optimal-control-based framework for trajectory planning, threat assessment, and semi-autonomous control of passenger vehicles in hazard avoidance scenarios," *Int. J. Vehicle Autonomous Systems*, vol. 8, no. 2/3/4, pp. 190–216, 2010.

[11] S. Anderson, S. Karumanchi, and K. Iagnemma, "Constraint-based planning and control for safe, semi-autonomous operation of vehicles," in *IEEE Intelligent Vehicles Symp.*, Alcalá de Henares, Spain, 2012, pp. 383–388.

[12] P. Sundström, M. Jonasson, J. Andreasson, A. Stensson Trigell, and B. Jacobsson, "Path and control optimisation for over-actuated vehicles in two safety-critical maneuvers," in *10th Int. Symp. on Advanced Vehicle Control (AVEC)*, Loughborough, United Kingdom, 2010.

[13] J. Andreasson, "Enhancing active safety by extending controllability — How much can be gained?" in *IEEE Intelligent Vehicles Symp.*, Xi'an, Shaanxi, China, June 2009, pp. 658–662.

[14] E. Schindler, *Fahrdynamik: Grundlagen Des Lenkverhaltens Und Ihre Anwendung Für Fahrzeugregelsysteme*. Renningen, Germany: Expert-Verlag, 2007.

[15] J. R. Ellis, *Vehicle Handling Dynamics*. London, United Kingdom: Mechanical Engineering Publications, 1994.

[16] H. B. Pacejka, *Tire and Vehicle Dynamics*, 2nd ed. Oxford, United Kingdom: Butterworth-Heinemann, 2006.

[17] U. Kiencke and L. Nielsen, *Automotive Control Systems—For Engine, Driveline and Vehicle*, 2nd ed. Berlin Heidelberg: Springer-Verlag, 2005.

[18] R. Rajamani, *Vehicle Dynamics and Control*. Berlin Heidelberg: Springer-Verlag, 2006.

[19] L. T. Biegler, A. M. Cervantes, and A. Wächter, "Advances in simultaneous strategies for dynamic process optimization," *Chemical Engineering Science*, vol. 57, pp. 575–593, 2002.

[20] Modelica Association, 2012, URL: http://www.modelica.org.

[21] J. Åkesson, "Optimica—an extension of Modelica supporting dynamic optimization," in *6th Int. Modelica Conf. 2008*. Modelica Association, Mar. 2008.

[22] J. Åkesson, K.-E. Årzén, M. Gäfvert, T. Bergdahl, and H. Tummescheit, "Modeling and optimization with Optimica and JModelica.org—Languages and tools for solving large-scale dynamic optimization problems," *Computers and Chemical Engineering*, Jan. 2010.

[23] JModelica.org, 2012, URL: http://www.jmodelica.org.

[24] A. Wächter and L. T. Biegler, "On the implementation of an interior-point filter line-search algorithm for large-scale nonlinear programming," *Mathematical Programming*, vol. 106, no. 1, pp. 25–57, 2006.